Monte Carlo simulation of CP^{N-1} models

Massimo Campostrini, Paolo Rossi, and Ettore Vicari
Dipartimento di Fisica dell'Università and Istituto Nazionale di Fisica Nucleare, I-56126 Pisa, Italy
(Received 2 April 1992)

Numerical simulations of two-dimensional CP^{N-1} models are performed at $N = 2$, 10, and 21. The lattice action adopted depends explicitly on the gauge degrees of freedom and shows precocious scaling. Our tests of scaling are the stability of dimensionless physical quantities (second moment of the correlation function versus inverse mass gap, magnetic susceptibility versus square correlation length) and rotation invariance. Topological properties of the models are explored by measuring the topological susceptibility and by extracting the Abelian string tension. Several different (local and nonlocal) lattice definitions of topological charge are discussed and compared. The qualitative physical picture derived from the continuum $1/N$ expansion is confirmed, and agreement with quantitative $1/N$ predictions is satisfactory. Variant (Symanzik-improved) actions are considered in the $CP^1 \approx O(3)$ case and agreement with universality and previous simulations (when comparable) is found. The simulation algorithm is an efficient mixture of over-heat-bath and microcanonical algorithms. The dynamical features and critical exponents of the algorithm are discussed in detail.

PACS numbers: 11.15 Ha, 11.15 Pg, 75.10 Hk

I. INTRODUCTION

Two-dimensional CP^{N-1} models take a special place in the realm of quantum field theory models, because of the close resemblance between many of their dynamical features and the properties expected to hold (but often very difficult to prove) in QCD. Among these properties we mention asymptotic freedom, spontaneous mass generation, unbroken gauge invariance, dynamical appearance of a linear confining potential between non-gauge-invariant states, and topological structure (instantons, anomalies, θ vacua).

CP^{N-1} models are however much easier to analyze because they involve spin instead of gauge fields and lower space dimensionality. Most properties of these models have been obtained in the context of the $1/N$ expansion [1–3]. It is however quite attractive to perform a numerical (Monte Carlo) analysis, in order to check the validity and range of applicability of the $1/N$ expansion and in order to explore the region of values of N where all analytical predictions are at best disputable.

Preliminary to all lattice simulations is the choice of a lattice action within the universality class of CP^{N-1} models. This choice, as well as the numerical algorithm, may be crucial to the purpose of minimizing the computational effort.

Theoretical considerations, supported by numerical evidence, led us to adopt a lattice action carrying an explicit dependence on the (Abelian) gauge degrees of freedom. The basic formulation [4–6] involves the action

$$S_{\mathrm{g}} = -\frac{1}{g}\sum_{n,\mu}\left(\bar{z}_{n+\mu}z_n\lambda_{n,\mu} + \bar{z}_n z_{n+\mu}\bar{\lambda}_{n,\mu} - 2\right),$$
$$g = \frac{1}{N\beta}, \tag{1}$$

where z_n is an N-component complex scalar field, constrained by the condition

$$\bar{z}_n z_n = 1 \tag{2a}$$

and $\lambda_{n,\mu}$ is a U(1) gauge field satisfying

$$\bar{\lambda}_{n,\mu}\lambda_{n,\mu} = 1\,. \tag{2b}$$

We also considered a Symanzik-improved [7] version of Eq. (1), involving next-to-nearest-neighbor interactions.

The gauge degrees of freedom are strongly fluctuating in the numerical simulation; therefore λ-dependent observables are hard to measure. In turn, all contributions to physical quantities are dominated by the lighter degrees of freedom that correspond to the continuum physics we are interested in. As a matter of fact, when comparing with the so-called standard action [5], we found precocious scaling, and for higher values of N even asymptotic scaling is observable.

We made an analytical effort to extend our continuum $1/N$ results [3] to the lattice version, along the lines discussed in Ref. [8]. The discussion of our methods and results and a comparison with numerical evaluations will be the subject of a separate paper in preparation.

It must however be said that quantitative agreement with the $1/N$ expansion can only be reached at very high values of N, because of the nonanalytic dependence on $1/N$ of the correlation length and of the very large coefficient in the effective expansion parameter $6\pi/N$ that can be easily extracted from a nonrelativistic Schrödinger-equation analysis of the linear confining potential [2, 3].

The purpose of the present paper is that of presenting numerical simulation results for CP^{N-1} models for rather different values of N.

On one side we studied $CP^1 \approx O(3)$. The formulation based on Eq. (1) is a not yet explored variant version of the model, that should however lay in the same universality class of the standard action and its Symanzik

counterpart [9, 10]. Comparing with previous literature on the subject, we found precocious scaling and agreement with universal results. The asymptotic m/Λ ratio predicted in Ref. [11] is however definitely beyond the region of couplings that can at present be numerically explored.

On the other side we performed preliminary, but rather complete and promising, numerical simulations of the CP^9 and CP^{20} models in order to measure the speed of approach to large-N asymptopia and check the continuity in N of the qualitative features of these models. Guided by previous analytic work on the subject, we decided to measure a wide choice of physical observables and explore possible alternative definitions.

A precondition for the lattice observability of a physical quantity is the requisite of group and gauge invariance. Therefore we considered the local gauge-invariant composite operator

$$P_{ij}(x) = \bar{z}_i(x) z_j(x) \tag{3}$$

and its group-invariant correlation function

$$G_P(x) = \langle \mathrm{Tr}\, P(x) P(0) \rangle_{\mathrm{conn}} \,. \tag{4}$$

We extracted the standard correlation length ξ_{w} from the long-distance behavior of the zero space momentum correlation function ("wall-wall" correlation), expected to behave like $\exp(-|x|/\xi_{\mathrm{w}})$. Moreover we introduced the "diagonal wall-wall" correlation length ξ_{d}, obtained by summing on the correlations between points located on two distinct parallel lines oriented at 45° with respect to the coordinate axes. The long-distance behavior is expected to be once more in the form $\exp(-|x|/\xi_{\mathrm{d}})$. The comparison between ξ_{w} and ξ_{d} offers us the possibility of a direct test of rotation invariance and, as a consequence, a measure of scaling deviations: the scaling region is characterized by $\xi_{\mathrm{w}} = \xi_{\mathrm{d}}$.

One cannot overstress the fact that, theoretically and for all numerical experiment purposes, tests of scaling are extremely more important than checks of asymptotic scaling. Asymptotic scaling is only needed to extract the Λ parameter of the lattice model. Moreover we do not expect this property to be accurately testable in the foreseeable future, with the exception of models such as CP^{N-1} at large N, where higher loop (nonuniversal) corrections to the beta function are very small.

An alternative definition of the correlation length comes from considering the second moment of the correlation function

$$\xi_G^2 = \frac{\int d^2x\, \frac{1}{4} x^2\, G_P(x)}{\int d^2x\, G_P(x)} \,. \tag{5}$$

In the scaling region the ratio ξ_G/ξ_{w} must be a constant, scale-independent number. There is however no reason for this number to be 1, or even N independent. Actually we showed that, defining the Λ parameter in terms of the perturbative ($1/N$ expandable) β function, the ratio ξ_G/Λ turns out to be an analytic function of $1/N$ around $N = \infty$, while ξ_{w}/Λ is nonanalytic, depending on the powers of $N^{-1/3}$. Moreover we predicted [12]

$$\frac{\xi_G}{\xi_{\mathrm{w}}} \to \sqrt{\frac{2}{3}} \tag{6}$$

when $N \to \infty$, while for $N = 2$ the ratio should be equal to 1 within 1%. The stability of ξ_G/ξ_{w} with respect to the coupling is another test of scaling, while its value measures how predictive the $1/N$ expansion may turn out to be.

Another class of interesting observables is related to the topological properties of the model. It is well known that, starting from the continuum definition of the topological charge density

$$q(x) = \frac{i}{2\pi}\, \varepsilon_{\mu\nu}\, \overline{D_\mu z}\, D_\nu z \,, \tag{7}$$

one can define a topological susceptibility

$$\chi_{\mathrm{t}} = \int d^2x\, q(x)\, q(0) \,. \tag{8}$$

Many lattice versions of $q(x)$ and χ_{t} have been proposed [13–17]. "Geometrical" definitions are nonlocal in the sense of quantum field theory and plagued (especially at low N) by the presence of "dislocations" that destroy the scaling behavior [13, 18]. On the other hand, local operator definitions unavoidably lead to mixing with lower and equal dimension operators and to the need of subtracting perturbative tails and performing finite renormalizations [19].

The theoretical predictions concerning the (scheme independent) value of the adimensional ratio $\chi_{\mathrm{t}}\xi^2$ are Lüscher's large-N result [20]

$$\chi_{\mathrm{t}}\xi_{\mathrm{w}}^2 = \frac{3}{4\pi N} + O\left(N^{-5/3}\right) \tag{9}$$

and our evaluation [12]

$$\chi_{\mathrm{t}}\xi_G^2 = \frac{1}{2\pi N}\left(1 - \frac{0.38}{N}\right) + O\left(\frac{1}{N^3}\right) . \tag{10}$$

Eqs. (9) and (10) are not in contradiction with each other, but the second one should be testable at lower values of N.

It is also possible to define the (Abelian) Wilson loop

$$W(\mathcal{C}) = \prod_{n,\mu \in \mathcal{C}} \lambda_{n,\mu} \,. \tag{11}$$

The physics of CP^{N-1} models leads to the prediction of an exponential area law behavior for sufficiently large Wilson loops:

$$W(\mathcal{C}) \sim e^{-\sigma A(\mathcal{C}) - \rho P(\mathcal{C})} \quad \text{for} \quad A(\mathcal{C}) \gg \xi^2 \,, \tag{12}$$

where σ is the Abelian string tension and ρ is a (renormalization-dependent) perimeter term. The ratio σ/χ_{t} is a pure number and its value is a scheme-independent quantity. It is easy to show that

$$\frac{\sigma}{2\pi^2 \chi_{\mathrm{t}}} = 1 + O\left(\frac{1}{N^2}\right) . \tag{13}$$

In principle one can also define the Polyakov line and study the correlation of two such lines, thus extracting the particle-antiparticle potential. In practice the sig-

nal is so small that one can hardly extract a physically meaningful number.

This paper is organized as follows.

In Sec. II the different lattice actions adopted for numerical simulations are presented and the physical observables are introduced together with their lattice definitions.

In Sec. III we present the details of our Monte Carlo algorithm with comments on its dynamical critical exponent and comparison between different approaches.

In Secs. IV and V we discuss specific features of the simulation for the CP^1 model and large-N CP^{N-1} models respectively and present the corresponding numerical results.

In Sec. VI problems related to the evaluation of the topological susceptibility in the CP^1 model are carefully analyzed.

In Sec. VII we comment on our numerical results and compare them with theoretical expectations.

In Sec. VIII we summarize our results and discuss their possible relevance in the general context of lattice field theories.

II. LATTICE DEFINITION OF OBSERVABLES

In order to evaluate a physical observable on the lattice, we need to choose an explicit definition in terms of lattice variables. This is especially true of the action. Most of our measurements were obtained by adopting either the action defined in Eq. (1),

$$S_{\rm g} = -N\beta \sum_{n,\mu} \left(\bar{z}_{n+\mu} z_n \lambda_{n,\mu} + \bar{z}_n z_{n+\mu} \bar{\lambda}_{n,\mu} - 2 \right), \tag{14}$$

or its Symanzik improved counterpart:

$$S_{\rm g}^{\rm Sym} = -N\beta \left[\frac{4}{3} \sum_{n,\mu} \left(\bar{z}_{n+\mu} z_n \lambda_{n,\mu} + \bar{z}_n z_{n+\mu} \bar{\lambda}_{n,\mu} - 2 \right) - \frac{1}{12} \sum_{n,\mu} \left(\bar{z}_{n+2\mu} z_n \lambda_{n,\mu} \lambda_{n+\mu,\mu} + \bar{z}_n z_{n+2\mu} \bar{\lambda}_{n,\mu} \bar{\lambda}_{n+\mu,\mu} - 2 \right) \right]. \tag{15}$$

We shall however make reference to the "standard" CP^{N-1} lattice action

$$S_1 = -N\beta \sum_{n,\mu} |\bar{z}_{n+\mu} z_n|^2 \tag{16}$$

and to its Symanzik improved version

$$S_1^{\rm Sym} = -N\beta \left[\frac{4}{3} \sum_{n,\mu} |\bar{z}_{n+\mu} z_n|^2 - \frac{1}{12} \sum_{n,\mu} |\bar{z}_{n+2\mu} z_n|^2 \right]. \tag{17}$$

It should be noticed that, in the case $N = 2$, Eqs. (16) and (17) can be rewritten in a O(3)-symmetric form by reexpressing the z fields in terms of

$$\mathbf{S}_n = \bar{z}_n \boldsymbol{\sigma} z_n \,, \tag{18}$$

reproducing the standard form of the action for the O(3) σ model and its Symanzik improved counterpart. We used this latter form of $S_1^{\rm Sym}$ as a variant action in the simulation of the CP^1 model.

In order to make contact with the continuum physics as described by the modified minimal subtraction ($\overline{\rm MS}$) renormalization scheme, we need to define a continuum $\Lambda_{\overline{\rm MS}}$ parameter and to evaluate the ratios of the different lattice Λ parameters to $\Lambda_{\overline{\rm MS}}$. The conventional definition of Λ is

$$\begin{aligned} \Lambda_{\overline{\rm MS}} &= \mu (b_0 g)^{-b_1/b_0^2} \exp\left(-\frac{1}{b_0 g} \right) \\ &= \mu \left(\frac{2\pi}{Ng} \right)^{2/N} \exp\left(-\frac{2\pi}{Ng} \right) \\ &= \mu (2\pi\beta)^{2/N} \exp(-2\pi\beta) \,. \end{aligned} \tag{19}$$

Evaluation of the ratios of Λ parameters is by now a rather standard exercise, involving the computation of the finite part of a one-loop Feynman integral. Let us only quote the results

$$\begin{aligned} \frac{\Lambda_{\overline{\rm MS}}}{\Lambda_{\rm g}} &= \sqrt{32} \exp\left(\frac{\pi}{2N} \right), \\ \frac{\Lambda_{\rm g}^{\rm Sym}}{\Lambda_{\rm g}} &= 1.345 \exp\left(\frac{0.444}{N} \right), \\ \frac{\Lambda_{\overline{\rm MS}}}{\Lambda_1} &= \sqrt{32} \exp\left(\frac{\pi}{2} \right), \\ \frac{\Lambda_1^{\rm Sym}}{\Lambda_1} &= 2.219 \,, \end{aligned} \tag{20}$$

implying also

$$\frac{\Lambda_{\rm g}}{\Lambda_1} = 2.193 \quad \text{for} \quad N = 2 \,. \tag{21}$$

We can introduce the gauge- and group-invariant correlation function $G_P(x,y)$ according to Eqs. (3) and (4). Let us now define the wall-wall correlation

$$G_{\rm w}(y-x) = \frac{1}{L} \sum_{x_1,y_1} G_P(x_1,x;\, y_1,y) \tag{22}$$

and the diagonal wall-wall correlation

$$G_{\rm d}\left(\frac{y-x}{\sqrt{2}} \right) = \frac{\sqrt{2}}{L} \sum_{x_1,y_1} G_P(x_1, x-x_1;\, y_1, y-y_1). \tag{23}$$

The expected large-distance behaviors, including periodic boundary condition effects, are

$$G_{\rm w}(x) \simeq \frac{A_{\rm w}}{2}\left[\exp\left(-\frac{x}{\xi_{\rm w}}\right)+\exp\left(-\frac{L-x}{\xi_{\rm w}}\right)\right] \quad \text{for} \quad \frac{L}{2} > x \gg \xi_{\rm w}\,, \tag{24}$$

$$G_{\rm d}(x) \simeq \frac{A_{\rm d}}{2}\left[\exp\left(-\frac{x}{\xi_{\rm d}}\right)+\exp\left(-\frac{L/\sqrt{2}-x}{\xi_{\rm d}}\right)\right] \quad \text{for} \quad \frac{L}{2\sqrt{2}} > x \gg \xi_{\rm d}\,. \tag{25}$$

In practice, $\xi_{\rm w}$, $\xi_{\rm d}$, $A_{\rm w}$, and $A_{\rm d}$ will be obtained by fitting the data for $G_{\rm w}$ and $G_{\rm d}$ by the functions (24) and (25), using all the values of x larger then a value $x_{\rm min}$ to be determined. In the scaling region, rotation invariance implies $\xi_{\rm w} = \xi_{\rm d}$ and $A_{\rm w} = A_{\rm d}$. Both $\xi_{\rm w}$ and $\xi_{\rm d}$ should reproduce in the continuum limit the inverse mass gap (denoted by $\overline{\xi}$ in [12]).

The correlation function $G_P(x)$ can be Fourier analyzed on a periodic lattice according to

$$\widetilde{G}_P(k) = \frac{1}{V}\sum_{x,y}\langle \mathrm{Tr}\, P(x)P(y)\rangle_{\rm conn} \exp\left[\frac{2i\pi}{L}(x-y)\cdot k\right]. \tag{26}$$

The zero component of $\widetilde{G}_P(k)$ is by definition the magnetic susceptibility $\chi_{\rm m}$. In the scaling region and in the small momentum regime we expect the behavior

$$\widetilde{G}_P(k) \approx \frac{Z_P}{\xi_G^{-2} + \sum_\mu 4\sin^2 \pi k_\mu/L}\,. \tag{27}$$

We can therefore use the two lowest components of $\widetilde{G}_P(k)$,

$$\chi_{\rm m} = \widetilde{G}_P(0,0) = Z_P\,\xi_G^2\,, \tag{28a}$$

$$\widetilde{G}_P(0,1) = \frac{Z_P}{\xi_G^{-2} + 4\sin^2 \pi/L}\,, \tag{28b}$$

to extract the following definition of ξ_G:

$$\xi_G^2 = \frac{1}{4\sin^2 \pi/L}\left[\frac{\widetilde{G}_P(0,0)}{\widetilde{G}_P(0,1)} - 1\right]. \tag{29}$$

In the scaling region, ξ_G defined by Eq. (29) should reproduce the corresponding continuum quantity (5) introduced in Ref. [12] (where it was denoted by ξ).

The quantity $Z_P = \chi_{\rm m}\xi_G^{-2}$ is obviously related to the renormalization of the composite operator P. Its dependence on β can therefore be determined by renormalization group considerations. One finds that

$$Z_P \sim g^{\gamma_1/b_0} \sim \beta^{-2}\,. \tag{30}$$

We therefore expect the combination $\beta^2\chi_{\rm m}\xi_G^{-2}$ to be approximately constant in the scaling region; in the large-N limit it can be evaluated analytically and turns out to be

$$\frac{\beta^2\chi_{\rm m}}{\xi_G^2} = \frac{3}{2\pi} + O\left(\frac{1}{N}\right). \tag{31}$$

Let us introduce the quantity $A_G = \chi_{\rm m}\xi_G^{-2}\xi_{\rm w}$. The adimensional ratio $A_{\rm w}/A_G$ is scheme independent in the scaling region. Standard field theory arguments lead to the relationship $A_{\rm w}/A_G \le 1$ for all N. We expect $A_{\rm w}/A_G \approx 1$ for CP^1 where the two-point function should be (almost) saturated by the lowest energy state. In the large-N limit $A_{\rm w}/A_G \to 0$, because the $\bar{z}z$ state becomes deconfined.

The geometrical definition of the topological charge was originally constructed in Ref. [6] in the form

$$q_n^{\rm g} = \frac{1}{2\pi}\,\mathrm{Im}\{\ln[\mathrm{Tr}\, P_{n+\mu+\nu}P_{n+\mu}P_n] + \ln[\mathrm{Tr}\, P_{n+\nu}P_{n+\mu+\nu}P_n]\}, \qquad \mu \neq \nu\,. \tag{32}$$

Introducing the quantity $\theta_{n,\mu} = \arg\{\bar{z}_n z_{n+\mu}\}$, one easily obtains

$$q_n^{\rm g} = \frac{1}{4\pi}\,\varepsilon_{\mu\nu}(\theta_{n,\mu} + \theta_{n+\mu,\nu} - \theta_{n+\nu,\mu} - \theta_{n,\nu})\,. \tag{33}$$

The absence of a perturbative tail for $q_n^{\rm g}$ has been explicitly verified in the $1/N$ expansion in [16].

The formulation (1) we adopted allows also for a local lattice representation not involving z fields, obtained by expressing the topological charge in terms of the gauge fields only. Let us define the plaquette operator (elementary Wilson loop)

$$U_{n,\mu\nu} = \lambda_{n,\mu}\lambda_{n+\mu,\nu}\bar{\lambda}_{n+\nu,\mu}\bar{\lambda}_{n,\nu}\,, \qquad U_n = U_{n,12} = \bar{U}_{n,21}\,. \tag{34}$$

The imaginary part of the plaquette U_n is a lattice representation of the topological charge density, and it will be denoted by $q_n^{(1)}$. Taking proper combinations of higher powers of the plaquette operator it is possible to construct an infinite sequence of local operators:

$$q_n^{(k)} = \sum_{l=1}^{k} \frac{(-1)^{l+1}}{l}\binom{2k}{k-l}\frac{2k}{\binom{2k}{k}}\,\mathrm{Im}(U_n)^l\,, \tag{35}$$

whose formal $k \to \infty$ limit leads to a geometrical definition of the topological charge. One can then construct the sequence of topological susceptibilities $\chi_{\rm t}^{(k)}$ obtained from $q_n^{(k)}$. Their (perturbatively evaluated) coefficients of mixing with other relevant operators involve, for high k, only very high powers of g. However the corresponding numerical weights are growing so fast with growing k that the convergence to the geometrical definition of $\chi_{\rm t}$ cannot be uniform. As a matter of fact, at fixed g an optimal value $\overline{k}$ exists such that the mixing is minimized. This phenomenon gives some theoretical support to the (numerically verified) notion that, especially at low N, geometrical definitions do not always reproduce the field theoretical predictions.

In the case of the CP^1 model, none of the definitions of topological charge discussed above is fully satisfactory for numerical simulations. We will discuss the alterna-

tive technique known as "field theoretical" method and related Monte Carlo results in Sec. VI.

Starting from the rectangular Wilson loops, we can define the Creutz ratios as

$$\chi(l,m) = \ln \frac{W(l,m-1)\,W(l-1,m)}{W(l,m)\,W(l-1,m-1)}. \tag{36}$$

The double ratio takes care of renormalization effects [constant and perimeter terms in $\ln W(l,m)$]. For $l,m \gg \xi$, we expect $\chi(l,m) \approx \sigma$.

The action S_g allows us to define improved estimators for operators that are linear with respect to each $\lambda_{n,\mu}$ variable, such as the Wilson loops. Improved estimators can be obtained by replacing each $\lambda_{n,\mu}$ with its average $\lambda^{\rm imp}_{n,\mu}$ in the field of its neighbors:

$$\begin{aligned}\lambda^{\rm imp}_{n,\mu} &= \frac{\int d\lambda_{n,\mu}\,\lambda_{n,\mu} \exp\left[2\beta N \,\mathrm{Re}\,(\bar z_{n+\mu} z_n \lambda_{n,\mu})\right]}{\int d\lambda_{n,\mu} \exp\left[2\beta N \,\mathrm{Re}\,(\bar z_{n+\mu} z_n \lambda_{n,\mu})\right]} \\ &= \frac{\bar z_{n+\mu} z_n}{|\bar z_{n+\mu} z_n|} \frac{I_1(2\beta N |\bar z_{n+\mu} z_n|)}{I_0(2\beta N |\bar z_{n+\mu} z_n|)},\end{aligned} \tag{37}$$

where I_0 and I_1 are modified Bessel functions. We used improved estimators wherever possible.

III. THE MONTE CARLO ALGORITHM

From the point of view of the Monte Carlo simulation, the action S_g defined in Eq. (1) offers remarkable advantages with respect to the standard formulation (that does not contain explicit gauge degrees of freedom). As we will show in the following sections, S_g enjoys precocious scaling and therefore simulations can be performed at relatively small correlation lengths and lattice sizes. Moreover, the introduction of an explicit λ field makes the action linear with respect to each lattice variable; therefore the action terms involving one z_n or $\lambda_{n,\mu}$ can be expressed as a scalar product of two real vectors. It is then easy to construct local algorithms containing overrelaxation procedures, such as the over-heat-bath [21] or the microcanonical algorithm [22], which are much more efficient than the standard Metropolis updating.

The sum of the terms involving z_n in the action S_g can be written as

$$s_z = -\beta N \,\mathrm{Re}\,\{\bar z_n \cdot F_{z,n}\}\,, \tag{38}$$

where $F_{z,n}$ is an N-component complex vector. Similarly the sum of the terms involving $\lambda_{n,\mu}$ is

$$s_\lambda = -\beta N \,\mathrm{Re}\,\{\bar\lambda_{n,\mu} F_{\lambda,n,\mu}\}\,, \tag{39}$$

where $F_{\lambda,n,\mu}$ is a complex number. By rewriting s_z and s_λ in terms of real vectors, doubling the number of components, we are left with the problem of updating a $2k$-component normalized real vector ϕ ($k = N$ for z, and $k = 1$ for λ) according to the action

$$s_\phi = -\beta N\, \phi \cdot F_\phi = -\beta N |F_\phi| \cos\theta\,, \tag{40}$$

where θ is the angle between ϕ and F_ϕ. We can generate a new angle $\theta^{\rm new}$ according to the probability distribution

$$dp_k(\cos\theta) = d\cos\theta\,(\sin\theta)^{2k-3} \exp(\beta N |F_\phi| \cos\theta)\,. \tag{41}$$

The algorithm used to generate θ according to (41) will be described in the Appendix.

In the over-heat-bath algorithm the remaining degrees of freedom of $\phi^{\rm new}$ are chosen according to the condition of minimizing the scalar product between $\phi^{\rm new}$ and $\phi^{\rm old}$. This condition is satisfied by taking

$$\phi^{\rm new} = \cos\theta^{\rm new} \frac{F_\phi}{|F_\phi|} - \left(\phi^{\rm old} - \cos\theta^{\rm old} \frac{F_\phi}{|F_\phi|}\right) \frac{\sin\theta^{\rm new}}{\sin\theta^{\rm old}}\,, \tag{42}$$

where $\theta^{\rm old}$ is the angle between $\phi^{\rm old}$ and F_ϕ, and $\theta^{\rm new}$ is the new angle generated according to (41). We obtain the upgraded lattice variable (z or λ) by reexpressing $\phi^{\rm new}$ as a complex vector. The over-heat-bath algorithm incorporates the requirements of a canonical distribution and of overrelaxation. Furthermore, it requires less computational effort than a standard heat bath.

Another overrelaxed algorithm can be obtained by alternating microcanonical and canonical updatings (the inclusion of canonical updatings is needed to ensure ergodicity). A microcanonical updating consists in choosing the new variable $\phi^{\rm new}$ that leaves the action unchanged but lies in the group space as far as possible from $\phi^{\rm old}$. This is achieved by setting $\theta^{\rm new} = \theta^{\rm old}$ in Eq. (42). In terms of the original variables we obtain

$$z^{\rm new} = 2 \frac{\mathrm{Re}\{z^{\rm old} \cdot F_z\}}{|F_z|^2} F_z - z^{\rm old}\,, \tag{43a}$$

$$\lambda^{\rm new} = 2 \frac{\mathrm{Re}\{\lambda^{\rm old} F_\lambda\}}{|F_\lambda|^2} F_\lambda - \lambda^{\rm old}\,. \tag{43b}$$

In order to check the efficiency of our overrelaxed algorithms, we used as a benchmark a Metropolis algorithm, which constructs the trial z variable by adding to the old z a random vector Δz and then projecting back to the original space of normalized vectors.

In Table I we report the computational time used by the different Monte Carlo algorithms to update the variables associated to one site (i.e., one z and two λ's), using the action S_g and its Symanzik improved counterpart, for several values of N. As expected, the computational time of the microcanonical algorithm increases linearly with

TABLE I. Computer time used by the different Monte Carlo algorithms to update the variables associated to one site. The unity of time is CPU μsec on a Cray/YMP.

N	Action	Algorithm	Time
10	S_g	Microcanonical	8.4
10	S_g	Over heat	19.7
10	S_g	2-hit Metropolis	19.2
10	$S_g^{\rm Sym}$	Microcanonical	18.6
10	$S_g^{\rm Sym}$	Over heat	29.9
21	S_g	Microcanonical	17.3
21	S_g	Over heat	29.0

N, and it is smaller than that of the over heat bath. The overhead of the over-heat-bath algorithm is essentially due to the generation of random numbers according to the distribution (41).

The best algorithm for reaching the equilibrium condition at a given β is the over heat bath, since it ensures a canonical distribution. Once the equilibrium is reached, a mixture of microcanonical and over heat bath is generally more efficient in decorrelating subsequent configurations, keeping into account the computational time. In all our runs we paid the utmost attention to thermalization, checking the stability of the average of each observable with respect to the number of thermalization sweeps.

The vectorization of our Monte Carlo simulation is achieved by dividing the lattice into blocks of size 3×3. We can update in parallel all the corresponding sites on different blocks even when using the Symanzik improved action. The mixture of the two algorithms is performed by choosing the procedure used to upgrade all the corresponding sites stochastically with a relative weight

$$\gamma = P_{\text{micro}}/P_{\text{over heat}} \tag{44}$$

(the choice is independent for the 9 classes of corresponding sites). We generally used $\gamma = 4$ in our simulations. The dynamical exponent z of our mixed algorithm will depend on γ: algorithms containing overrelaxation procedures can show very different dynamical behavior, and only an optimized overrelaxation can give a critical dynamical exponent $z \simeq 1$, which represents the free-field limit investigated by Adler [23]. A similar problem for the case of the O(3) σ model with the standard lattice action was analyzed in Ref. [19].

In order to test the performance of these algorithms, we calculated the integrated autocorrelation time $\tau_{\chi_{\text{m}}}$ of the normalized autocorrelation function $A(t)$ of the magnetic susceptibility χ_{m}:

$$\tau_{\chi_{\text{m}}} = \tfrac{1}{2}\sum_{t=-\infty}^{\infty} A(t)\,,$$
$$A(t) = \frac{\sum_{n=1}^{M}[\chi_{\text{m}}(n+t)-\overline{\chi}_{\text{m}}][\chi_{\text{m}}(n)-\overline{\chi}_{\text{m}}]}{\sum_{n=1}^{M}[\chi_{\text{m}}(n)-\overline{\chi}_{\text{m}}]^2}\,, \tag{45}$$

where $\chi_{\text{m}}(n)$ is χ_{m} measured on the nth configuration, M is the total number of thermalized configurations, and $\overline{\chi}_{\text{m}}$ is the average over the M configurations. A self-consistent truncation window of width $4\times\tau$ was employed to estimate $\tau_{\chi_{\text{m}}}$ (cf. [24]). In Table II we report the autocorrelation times of the magnetic susceptibility obtained from the simulation of the CP^{N-1} models with action S_{g}, using the mixture of algorithms with $\gamma = 4$. We determine a dynamical critical exponent from the data: $\tau_{\chi_{\text{m}}}$ is expected to behave asymptotically as $\tau_{\chi_{\text{m}}} \simeq c\xi^z$, where c and z depend on the algorithm employed and on N, but not on β. In Fig. 1 a log-log plot of $\tau_{\chi_{\text{m}}}$ versus ξ_G is shown. A best fit to the data gives

$$z = 1.39(5), \quad c = 0.96(7) \quad \text{for } N = 2\,, \tag{46a}$$
$$z = 1.26(5), \quad c = 0.88(6) \quad \text{for } N = 10 \tag{46b}$$

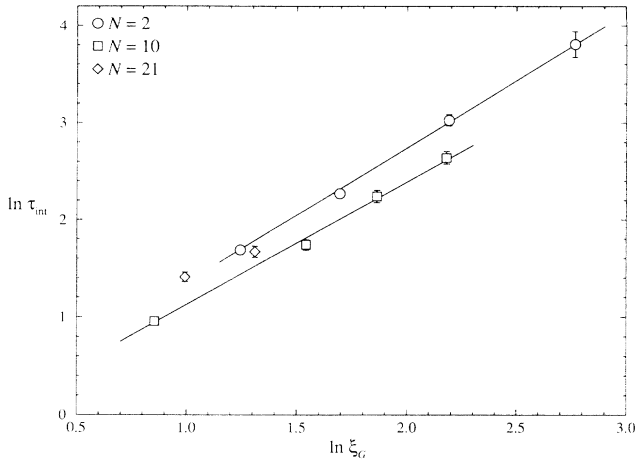

FIG. 1. Autocorrelation of the magnetic susceptibility. The solid lines are fits to the dynamical exponents.

(the values for $N = 10$ are probably affected by finite size effects; the infinite lattice value of z should be slightly lower). The values of $\tau_{\chi_{\text{m}}}$ for CP^{20} are close to the corresponding values for CP^1 and CP^9, and we therefore expect z to be in the same range; however, our data are insufficient to obtain a precise determination of z and c.

Our algorithm is much more efficient than the 2-hit Metropolis algorithm (tuned to 50–60% acceptance): the efficiency is improved by about two orders of magnitude already for a correlation length $\xi \simeq 5$.

The dynamical critical exponent z of the Monte Carlo algorithms for spin models is usually determined by measuring the autocorrelation times of the magnetic susceptibility, because χ_{m} is expected to couple strongly with the longest and slowest modes. We found that this is not completely true at high N. Indeed in our simulations the topological susceptibility showed not only the longest autocorrelations but also a different (and slower) dynamical behavior.

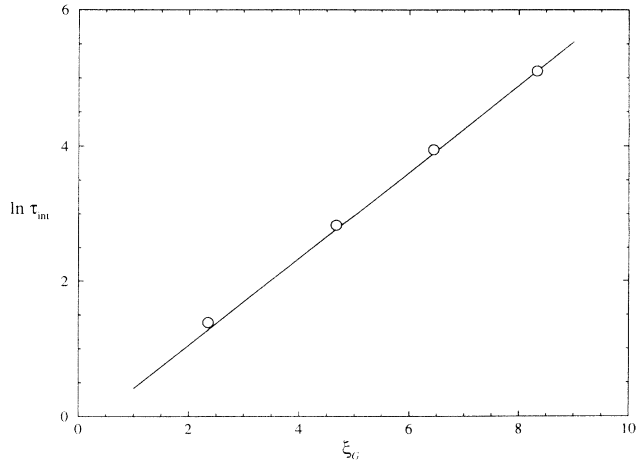

FIG. 2. Autocorrelation of the topological susceptibility for CP^{20}. The solid line is an exponential fit.

TABLE II. Autocorrelation time of the magnetic and topological susceptibility.

N	L	β	ξ_G	L/ξ_G	$\tau_{\rm int}^{\chi_m}$	$\tau_{\rm int}^{\chi_t}$
2	24	1.1	3.47(2)	6.91(4)	5.4(1)	—
2	54	1.2	5.45(11)	9.9(2)	9.7(4)	—
2	60	1.3	8.93(18)	6.7(1)	20.6(1.2)	—
2	120	1.4	15.9(8)	7.6(4)	45(6)	—
10	42	0.7	2.35(3)	17.87(23)	2.6(1)	4
10	60	0.8	4.68(5)	12.83(13)	5.7(3)	17
10	72	0.85	6.44(6)	11.18(10)	9.4(6)	52
10	90	0.9	8.83(7)	10.19(8)	14.0(9)	164
21	36	0.65	2.70(1)	13.33(5)	4.1(2)	63
21	48	0.7	3.71(2)	12.94(7)	5.3(3)	—

The determination of the autocorrelation function requires the measurement of the relevant observable for each updating sweep; this is far too expensive in the case of the topological susceptibility χ_t. Therefore we estimated the integrated autocorrelation time τ_{χ_t} by studying the behavior of the error of χ_t under the blocking procedure employed to control autocorrelation effects. An estimate of τ_{χ_t} can be obtained through the relationship

$$\tau_{\chi_t} \simeq \frac{I}{2}\left(\frac{E}{E_0}\right)^2, \tag{47}$$

where I is the number of sweeps between two measurements, E_0 is the naive error calculated without taking into account the autocorrelations, and E is the correct error found after the blocking procedure (the estimate is meaningful only if $I < \tau_{\chi_t}$). In Table II we report the estimated values of τ_{χ_t}. In Fig. 2 a log plot of τ_{χ_t} versus ξ_G for the CP^{20} model is shown, displaying a behavior $\tau_{\chi_t} \sim \exp(a\xi)$. On the other hand, we observed for the autocorrelation times of the Wilson loops a power law behavior, very similar to the behavior (46) of τ_{χ_m}. We repeated the evaluation of τ_{χ_m} using this method, and found results consistent with the direct measure by Eq. (45).

In Ref. [25] a multigrid algorithm was presented for the CP^{N-1} models, which eliminates critical slowing down ($z \simeq 0$). However, the good scaling properties of the action S_g allowed us to work at small correlation lengths and lattice sizes, where the local overrelaxed algorithm is expected to be more efficient than any multiscale algorithm.

IV. SIMULATIONS OF CP^1

We performed Monte Carlo simulations of the CP^1 model in the basic formulation (1) for several values of β corresponding to correlation lengths ξ up to 20 lattice units. We also simulated two Symanzik improved formulations, corresponding to S_g (15) and to the standard formulation S_1 (17) respectively. A summary of the runs is presented in Table III. We use here and in the following the notation "ov" for over-heat-bath updating, and "m,γ" for a stochastic mixture of microcanonical and over-heat-bath updating with ratio γ [cf. (44)].

The data for the different definitions of correlation length and of correlation function coefficient are reported in Table IV, for the largest lattice simulated at each β. The fits to G_w and G_d were performed choosing $x_{\rm min} \approx \xi_w$; fits using a larger $x_{\rm min}$ gave consistent results: this stability is to be expected, since the spectrum of the CP^1 model has only one particle. The ratios of these different definitions, analyzed using the jackknife method, are reported in Table V. The data show scaling and rotation invariance (within statistical errors of about 1%) even for the smallest value of $\xi \approx 3.5$.

Table VI shows that the quantity $\beta^2\chi_m\xi_G^{-2}$ is constant within our range of β, as predicted by the renormaliza-

TABLE III. Summary of the simulation runs for the CP^1 model. Asterisks mark runs for the Symanzik improved action (15). Degree marks runs for the Symanzik improved action (17).

β	L	Stat	E	ξ_G	χ_m	$\tau_{\rm int}^{\chi_m}$
1.1	12	200k m,4	0.5528(3)	3.283(14)	11.14(5)	4.6(1)
1.1	15	400k m,4	0.55480(16)	3.400(10)	11.99(4)	4.9(1)
1.1	18	400k m,4	0.55581(14)	3.438(14)	12.36(5)	5.1(1)
1.1	21	400k m,4	0.55599(13)	3.477(17)	12.51(5)	5.4(1)
1.1	24	400k m,4	0.55596(11)	3.473(20)	12.55(5)	5.4(1)
1.1	36	100k m,3	0.55593(14)	3.48(7)	12.62(12)	5.7(2)
1.2	54	100k m,4	0.49559(10)	5.45(11)	26.2(3)	9.7(4)
1.3	27	100k m,4	0.44380(19)	8.33(7)	51.5(4)	11.5(5)
1.3	36	100k m,4	0.44496(16)	8.70(10)	57.3(6)	16.7(9)
1.3	45	100k m,4	0.44487(11)	8.77(12)	59.3(8)	18.9(1.0)
1.3	60	100k m,4	0.44494(8)	8.93(18)	61.0(9)	20.6(1.2)
1.4	120	50k m,4	0.40367(8)	15.9(9)	162(5)	~ 45
1.45	150	50k m,1	0.38601(6)	21.2(1.1)	269(10)	~ 50
1.0 *	36	100k m,4	0.59252(14)	3.84(7)	15.77(15)	6.9(2)
1.1 *	54	100k m,4	0.52402(7)	5.93(15)	33.2(4)	13.7(6)
1.1 °	36	100k ov	1.1186(3)	4.05(5)	17.10(13)	3.9(1)
1.2 °	54	100k ov	1.0038(2)	5.87(10)	33.1(3)	7.4(3)

TABLE IV. Correlation length ξ and correlation function coefficient A for the CP^1 model.

β	L	ξ_G	ξ_w	ξ_d	A_G	A_w	A_d
1.1	36	3.48(7)	3.50(7)	3.52(7)	3.64(6)	3.57(7)	3.52(7)
1.2	54	5.45(11)	5.45(11)	5.47(9)	4.82(8)	4.76(11)	4.77(8)
1.3	60	8.93(18)	8.89(23)	9.07(14)	6.81(7)	6.88(17)	6.73(5)
1.4	120	15.9(9)	15.9(7)	15.6(7)	10.1(5)	10.2(5)	10.5(4)
1.45	150	21.2(1.1)	21.7(1.4)	21.5(1.1)	13.0(5)	12.3(8)	12.5(5)
1.0 *	36	3.84(7)	3.86(7)	3.85(5)	4.12(5)	4.03(7)	4.07(5)
1.1 *	54	5.93(15)	5.95(16)	5.94(12)	5.63(9)	5.60(14)	5.62(8)
1.1 °	36	4.05(5)	4.07(5)	4.02(5)	8.46(8)	8.27(11)	8.45(8)
1.2 °	54	5.87(10)	5.90(10)	6.04(9)	11.33(14)	11.26(18)	10.85(12)

tion group. Table VI includes also a test of asymptotic scaling [according to the two-loop beta function $f(\beta) = 2\pi\beta e^{-2\pi\beta}$], reporting the quantity $M_G/\Lambda_g = [\xi_G f(\beta)]^{-1}$. For the Symanzik improved actions, Λ_g is obtained by use of Eq. (20).

The runs reported here were also used to measure the topological susceptibility by the "field theoretical" method. We will present the results in Sec. VI.

The data taken on lattices of different size for $\beta = 1.1$ and $\beta = 1.3$ can be used to test the predictions of finite size scaling for the observables ξ_G and χ_m. Since we used values of the finite size scaling parameter $z = L/\xi_G$ bigger than 3, we can fit our data at fixed β to the formula

$$\frac{O_L}{O_\infty} = f_O(z) = 1 + c_O e^{-z}, \tag{48}$$

where O is ξ_G or χ_m. Equation (48) fits very well the data. The results are shown in Table VII. The values of c_O obtained from fits at different β are compatible. O_∞ obtained from the fit can be used to compute the finite size scaling function $f_O(z)$. f_{ξ_G} is plotted in Fig. 3; f_{χ_m} is plotted in Fig. 4.

V. SIMULATIONS OF CP^{N-1} FOR LARGE N

We performed Monte Carlo simulations of the CP^9 model in the basic formulation (1) and in the corresponding Symanzik improved formulation (15) for several values of β corresponding to correlation lengths ξ up to 9 lattice units. The runs are summarized in Table VIII.

TABLE V. Ratios of different definitions of correlation length and correlation function coefficient for the CP^1 model.

β	L	ξ_G/ξ_w	ξ_d/ξ_w	A_w/A_G	A_d/A_w
1.1	36	0.995(8)	1.008(13)	0.981(17)	0.986(21)
1.2	54	1.000(7)	1.003(14)	0.987(17)	1.002(24)
1.3	60	1.004(9)	1.020(16)	1.013(27)	0.977(24)
1.4	120	1.00(3)	0.98(4)	1.00(8)	1.03(6)
1.45	150	0.98(3)	0.99(5)	0.95(7)	1.02(7)
1.0 *	36	0.996(5)	0.997(10)	0.979(12)	1.009(17)
1.1 *	54	0.997(7)	0.999(14)	0.995(20)	1.003(23)
1.1 °	36	0.996(4)	0.988(9)	0.977(11)	1.022(14)
1.2 °	54	0.995(6)	1.023(11)	0.994(15)	0.964(17)

The data for the different definitions of correlation length and of correlation function coefficient are reported in Table IX, for the largest lattice simulated at each β. The fits to G_w and G_d were performed choosing $x_{min} \approx 2\xi_w$. Fits using a larger x_{min} gave consistent results, but fits using $x_{min} < 2\xi_w$ showed a clear difference: this is a consequence of the complex particle spectrum of the model. The ratios of these different definitions are reported in Table X. The data show scaling and rotation invariance (within statistical errors of about 1%) even for the smallest value of $\xi \approx 3$.

Figure 5 shows the rescaled square Creutz ratios $\chi(l,l)\xi_G^2$, plotted as a function of the physical distance $r = l/\xi_G$, for several values of β. Universality of this adimensional function is very clear from the data. However it is difficult to extract unambiguously a value for the string tension without a major increase of our statistics. The best we can do is to quote the value of σ estimated from a single value of $\chi(l,l)$; the results are presented in Table XI.

$\beta^2\chi_m\xi_G^{-2}$ is shown in Table XII. Table XII includes also a test of asymptotic scaling [according to the two-loop beta function $f(\beta) = (2\pi\beta)^{1/5}e^{-2\pi\beta}$], reporting the quantity $M_G/\Lambda_g = [\xi_G f(\beta)]^{-1}$. For the Symanzik improved action, Λ_g is obtained by use of Eq. (20).

The topological susceptibility χ_t^g measured using the geometrical definition (32) is shown in Table XII. We also measured χ_t^k using the local definitions (35), up to $k = 3$, and found results consistent with χ_t^g. We measured χ_t^g on lattices of different size and verified that finite size effects are under control.

TABLE VI. Further results for the CP^1 model.

β	L	$\beta^2\chi_m\xi_G^{-2}$	M_G/Λ_g
1.1	36	1.26(7)	41.7(8)
1.2	54	1.27(6)	45.8(1.5)
1.3	60	1.29(4)	48.3(1.0)
1.4	120	1.26(9)	47.2(2.7)
1.45	150	1.26(9)	46.9(2.4)
1.0 *	36	1.07(5)	37.3(7)
1.1 *	54	1.14(6)	41.1(1.0)
1.1 °	36	1.26(3)	36.3(5)
1.2 °	54	1.38(4)	43.0(7)

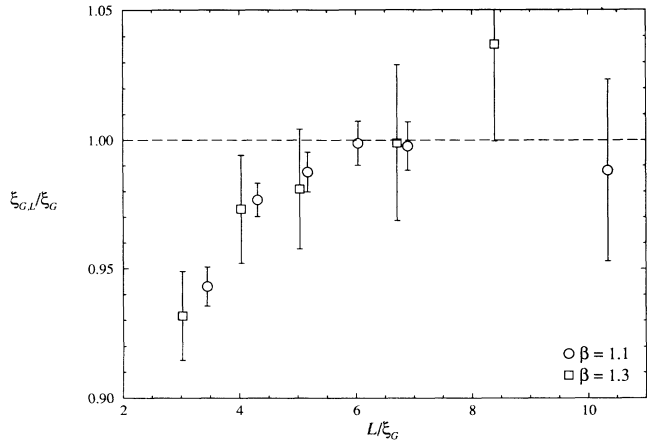

FIG. 3. Finite size scaling of the correlation length ξ_G for the CP^1 model.

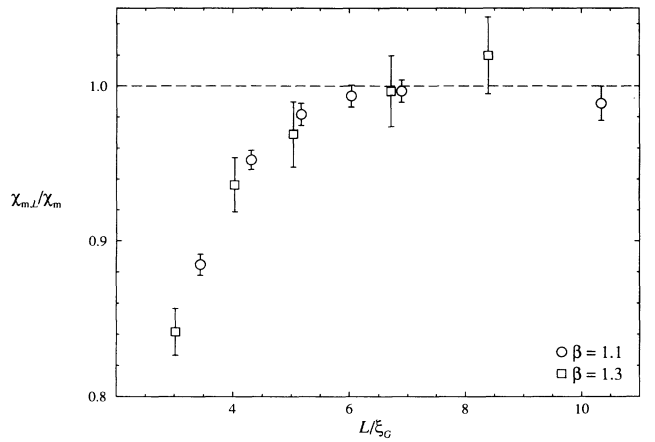

FIG. 4. Finite size scaling of the magnetic susceptibility χ_m for the CP^1 model.

TABLE VII. Finite size scaling fits for the CP^1 model.

O	β	O_∞	c_O	χ^2/N_{DF}
ξ_G	1.1	3.481(13)	−1.7(4)	0.3
ξ_G	1.3	8.89(9)	−1.3(3)	0.3
χ_m	1.1	12.59(4)	−3.5(3)	0.8
χ_m	1.3	60.8(5)	−3.2(2)	0.4

We simulated the CP^{20} model only in the basic formulation (1), for values of β corresponding to correlation lengths ξ up to 5 lattice units. The runs are summarized in Table XIII.

The data for the different definitions of correlation length and of correlation function coefficient are reported in Table XIV, for the largest lattice simulated at each β. The fits to G_w and G_d were performed choosing $x_{min} \approx 2\xi_w$. The ratios of these different definitions are reported in Table XV.

The rescaled square Creutz ratios $\chi(l,l)\xi_G^2$ are plotted as a function of $r = l/\xi_G$ in Fig. 6. The values of the string tension σ estimated from $\chi(l,l)$ are presented in Table XVI.

Table XVII displays $\beta^2\chi_m\xi_G^{-2}$ and the test of asymptotic scaling [according to the two-loop beta function $f(\beta) = (2\pi\beta)^{2/21}e^{-2\pi\beta}]$ $M_G/\Lambda_g = [\xi_G f(\beta)]^{-1}$.

The topological susceptibility measured for $\beta = 0.65$ using the geometrical definition is also reported in Table XVII. The exponential growth of the autocorrelation time τ_{χ_t} (discussed in Sec. III) prevented us from obtaining meaningful measurements of χ_t for higher values of β. However, the autocorrelation time of all the other observables is under control and their measurements are correct, because the relevant degrees of freedom decouple at large N from the topological ones.

The $1/N$ expansion predicts a radius of the ground state proportional to $\xi N^{1/3}$. We can therefore expect that, for large enough N, finite size effects are dominated by the size of the ground state and not by its mass. In

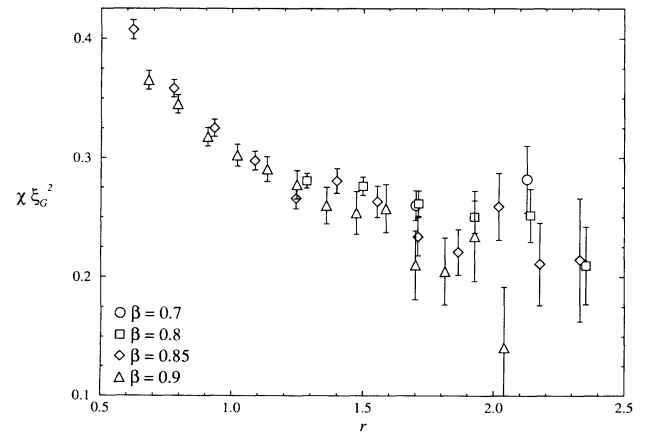

FIG. 5. Creutz ratios $\chi(l,l)$, rescaled according to the correlation length ξ_G, as a function of the physical distance $r = l/\xi_G$ for the CP^9 model.

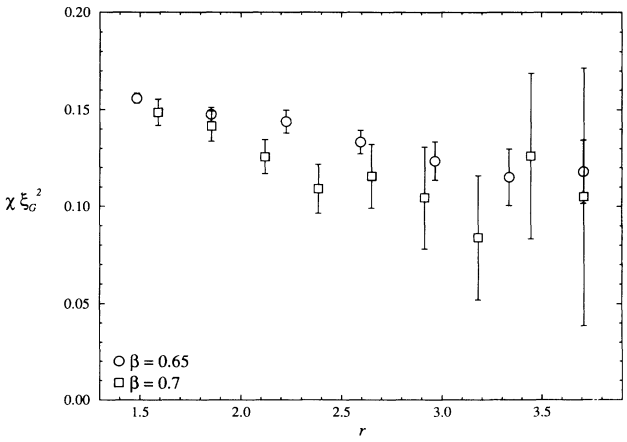

FIG. 6. Creutz ratios $\chi(l,l)$, rescaled according to the correlation length ξ_G, as a function of the physical distance $r = l/\xi_G$ for the CP^{20} model.

TABLE VIII. Summary of the simulation runs for the CP^9 model. Asterisks mark runs for the Symanzik improved action (15).

β	L	Stat	E	ξ_G	χ_m	$\tau_{int}^{\chi m}$
0.7	42	40k m,4	0.78402(13)	2.35(3)	10.20(3)	2.6(1)
0.8	27	40k m,4	0.66501(20)	5.18(3)	32.14(21)	14.7(1.1)
0.8	30	40k m,4	0.66591(17)	5.07(4)	31.07(23)	14.9(1.2)
0.8	36	40k m,4	0.66695(15)	4.71(4)	28.79(18)	10.3(7)
0.8	48	40k m,4	0.66668(11)	4.59(4)	28.23(13)	6.8(4)
0.8	60	40k m,1	0.66701(8)	4.67(5)	28.27(11)	5.6(3)
0.85	48	60k m,4	0.62196(9)	6.63(5)	48.73(32)	18.2(1.3)
0.85	60	40k m,4	0.62216(8)	6.48(5)	47.41(26)	12.1(9)
0.85	72	40k m,4	0.62214(8)	6.44(6)	47.18(22)	9.4(6)
0.9	60	50k m,4	0.58354(9)	9.33(11)	83.3(7)	28.7(2.8)
0.9	90	50k m,4	0.58373(5)	8.83(8)	78.5(4)	14.0(9)
0.7 *	42	40k m,4	0.75714(11)	3.81(2)	23.37(8)	5.9(3)
0.75 *	60	40k m,4	0.70115(7)	5.17(4)	37.52(14)	7.3(4)

order to test both the predictions of finite size scaling and of $1/N$ expansion, we performed a finite size analysis using the finite size scaling parameter $v = L\xi_G^{-1}N^{-1/3}$.

The finite size scaling functions f_{ξ_G} and f_{χ_m} were obtained by approximating infinite lattice quantities with the corresponding values measured on the largest lattice available for each β and N. f_{ξ_G} and f_{χ_m} are plotted as functions of v in Figs. 7 and 8 respectively, including data both for the CP^9 and for the CP^{20} model.

We performed a global fit to our data with the formula

$$\frac{O_L}{O_\infty} = f_O = 1 + c_O \exp\left(-\frac{v}{d_O}\right), \tag{49}$$

including both CP^9 and CP^{20} data. The results are

$$d_{\xi_G} = 0.47(5), \quad c_{\xi_G} = 41(26), \quad \chi^2/N_{DF} = 0.9, \tag{50a}$$

$$d_{\chi_m} = 0.50(3), \quad c_{\chi_m} = 32(11), \quad \chi^2/N_{DF} = 0.9. \tag{50b}$$

VI. TOPOLOGICAL SUSCEPTIBILITY OF THE CP^1 MODEL

In the two-dimensional (2D) O(3) σ model or CP^1 model, geometrical definitions of topological charge are plagued by the presence of dislocations [6, 13], i.e., topological structures of the size of one lattice spacing whose unphysical contribution to χ_t does not vanish in the continuum limit. As a consequence, the topological susceptibility derived from these definitions does not show the expected scaling behavior. An alternative approach, that is not affected by dislocations, relies on a definition of topological charge density by a local polynomial in the lattice variables. Local operator definitions are subject to mixing with lower and equal dimension operators and to finite renormalizations. We used this approach to determine χ_t in the CP^1 model.

On the lattice a topological charge density operator having the correct classical continuum limit $q^L(x) \to a^2 q(x) + O(a^4)$ (a being the lattice spacing) can be defined as

$$q^L(x) = -\frac{i}{2\pi}\sum_{\mu\nu}\epsilon_{\mu\nu}\mathrm{Tr}\left[P(x)\Delta^s_\mu P(x)\Delta^s_\nu P(x)\right], \tag{51}$$

where Δ^s is a symmetrized version of the finite derivative:

$$\Delta^s_\mu P(x) = \tfrac{1}{2}[P(x+\mu) - P(x-\mu)]. \tag{52}$$

In order to determine χ_t, the correlation at zero momentum of two $q^L(x)$ operators χ_t^L is calculated:

$$\chi_t^L = \left\langle \sum_x q^L(x) q^L(0) \right\rangle = \frac{1}{V}\left\langle \left(Q^L\right)^2 \right\rangle, \tag{53a}$$

$$Q^L = \sum_x q^L(x). \tag{53b}$$

χ_t^L is connected to χ_t by a nontrivial relationship, since the presence of irrelevant operators of higher dimension in $q^L(x)$ induces quantum corrections. The classical continuum limit of $q^L(x)$ must be corrected including

TABLE IX. Correlation length ξ and correlation function coefficient A for the CP^9 model.

β	L	ξ_G	ξ_w	ξ_d	A_G	A_w	A_d
0.7	42	2.35(3)	2.42(2)	2.43(3)	4.46(6)	3.90(8)	3.89(9)
0.8	60	4.67(5)	4.88(6)	4.81(6)	6.32(7)	5.29(14)	5.49(13)
0.85	72	6.44(6)	6.69(10)	6.75(9)	7.62(8)	6.56(20)	6.47(16)
0.9	90	8.83(8)	9.07(10)	9.07(11)	9.14(9)	8.28(21)	8.25(18)
0.7 *	42	3.81(2)	3.93(4)	3.93(3)	6.34(3)	5.63(12)	5.64(7)
0.75 *	60	5.17(4)	5.28(9)	5.30(6)	7.42(5)	6.83(23)	6.77(13)

TABLE X. Ratios of different definitions of correlation length and correlation function coefficient for the CP^9 model.

β	L	ξ_G/ξ_w	ξ_d/ξ_w	A_w/A_G	A_d/A_w
0.7	42	0.971(6)	1.003(8)	0.874(15)	0.996(20)
0.8	60	0.957(8)	0.984(12)	0.837(26)	1.037(33)
0.85	72	0.962(10)	1.009(14)	0.861(33)	0.987(35)
0.9	90	0.973(9)	0.999(13)	0.905(29)	0.997(33)
0.7 *	42	0.968(6)	1.000(7)	0.887(21)	1.002(18)
0.75 *	60	0.979(9)	1.005(11)	0.922(35)	0.990(28)

a renormalization constant $Z(\beta)$ [26]. Other contributions originate from contact terms, i.e., from the limit $x \to 0$ in Eq. (53). These contact terms appear as mixings with the trace of the energy-momentum tensor $S(x)$ and with the identity operator I, which are the only available operators with equal or lower dimension. Therefore the relationship between the lattice and the continuum topological susceptibility takes the form

$$\chi_t^L(\beta) = a^2 Z(\beta)^2 \chi_t + a^2 A(\beta)\langle S(x)\rangle_{np} + P(\beta)\langle I\rangle + O(a^4) . \tag{54}$$

np denotes the nonperturbative part (i.e., the perturbative tail must be subtracted). $Z(\beta)$, $P(\beta)$, and $A(\beta)$ are ultraviolet effects, since they originate from the ultraviolet cutoff-dependent modes. They can be computed in perturbation theory as series in β^{-1}.

In the following we will neglect the contribution of the mixing with $S(x)$. This assumption is supported by a perturbative argument: the perturbative series of $A(\beta)$ starts with a β^{-3} term. This assumption will be further supported by the consistency of the final results.

In order to estimate the renormalization functions in Eq. (54) nonperturbatively, we applied the method proposed in Ref. [27]. We start from a configuration C_0 carrying a definite topological charge Q_0 which is an approximate minimum of the lattice action (in this sense we will call it a "classical" configuration). We heat

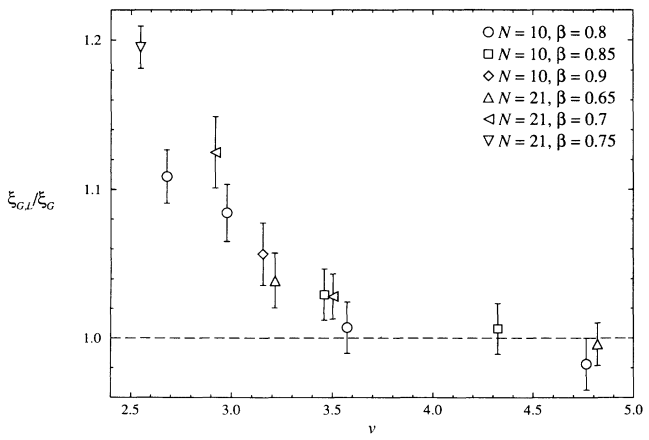

FIG. 7. Finite size scaling of the correlation length ξ_G for the CP^9 and CP^{20} models.

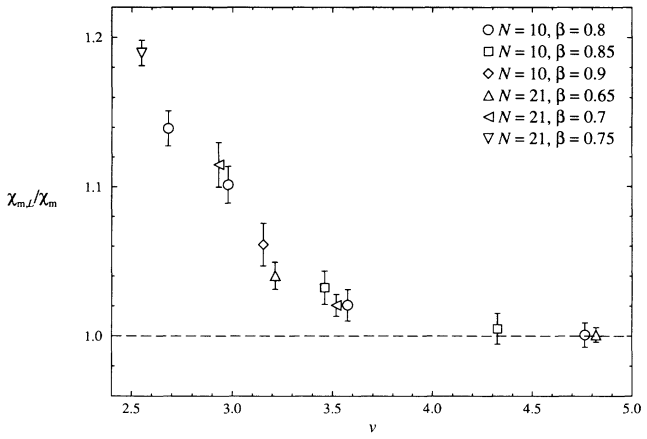

FIG. 8. Finite size scaling of the magnetic susceptibility χ_m for the CP^9 and CP^{20} models.

it by a local updating procedure in order to introduce short-ranged fluctuations, taking care to leave intact the background topological structure. We construct ensembles $\mathcal{C}_n^{(Q_0)}$ of many independent configurations obtained by heating the starting configuration C_0 for the same number n of updating steps, and average the topological charge over the ensembles. If $\xi \gg a$, there should exist an intermediate range of n where fluctuations of length $l \sim a$ are thermalized at the given value of β and reproduce the renormalization effects, while fluctuations at the scale $l \sim \xi$ are off equilibrium and still determined by the initial configuration. The average of $q^L(x)$ over the configurations in this range of n should be approximately equal to $Z(\beta)\, Q_0$.

We can also start from a constant configuration (with $Q_0 = 0$) and construct other ensembles $\mathcal{C}_n^{(0)}$ of configurations. We should find an intermediate region of n where the measure of χ_t^L gives an estimate of the mixing $P(\beta)$ with the identity operator which, being a short-ranged effect (due to the fluctuations at $l \sim a$), is expected to be independent of the physical topological background structure.

If we plot the values $q^L(x)$ averaged over $\mathcal{C}_n^{(Q_0)}$ and the values of χ_t^L averaged over $\mathcal{C}_n^{(0)}$ as functions of n, we should observe plateaus in correspondence of the above-mentioned intermediate ranges. The characteristics (starting point and length) of the plateaus are determined by the phenomenon of critical slowing down. The renormalization functions are determined by short-ranged fluctuations, which we do not expect to be critically slowed down; therefore the starting point of the plateaus should be independent of β. On the other hand, the end point of the plateaus is reached when the Monte Carlo procedure changes the long-ranged modes that determine the topological properties, and critical slowing down should strongly affect these modes; therefore the length of the plateaus should be β dependent. This behavior is essential for the existence of an intermediate range of n where the renormalization effects can be measured: indeed the success of the present method for esti-

TABLE XI. The string tension obtained from the Creutz ratio $\chi(l,l)$ for the CP^9 model.

β	L	l	$10^3\sigma$	$\sigma\xi_G^2$	l	$10^3\sigma$	$\sigma\xi_G^2$
0.7	42	4	47(2)	0.260(12)	5	51(5)	0.28(3)
0.8	60	8	12.0(4)	0.261(11)	10	11.5(1.0)	0.25(2)
0.85	72	10	6.3(3)	0.263(12)	13	6.2(7)	0.26(3)
0.9	90	14	3.3(3)	0.257(20)	17	3.0(5)	0.23(4)
0.7 *	42	6	15(2)	0.22(3)	8	16(7)	0.23(10)
0.75 *	60	8	11(2)	0.29(6)	10	4(6)	—

mating $Z(\beta)$ and $P(\beta)$ strongly relies on the distinction between the fluctuations at distance $l \sim a$, contributing to the renormalizations, and those at $l \sim \xi$ determining the relevant topological properties. The fluctuations at $l \sim a$ are soon thermalized, whereas the topological charge thermalization is much slower.

In order to check that heating does not change the background topological structure of the initial configuration, after a given number of heating sweeps we cool the configurations (by locally minimizing the action) and verify that the cooled configurations have topological charge equal to Q_0.

We used as an updating procedure a 10-hit Metropolis algorithm (tuned to 50–60% acceptance), which gives a sufficiently mild heating. In order to obtain reliable estimates of the renormalization functions, we found it necessary to use correlation lengths bigger than 10–15 lattice spacings.

We construct the initial configuration carrying topological charge $Q_0 = 1$ ("lattice instanton") starting from a discretization of the continuum SU(2) instanton:

$$
\begin{aligned}
z_1(x) &= \frac{x_1 - \bar{x}_1 - i(x_2 - \bar{x}_2)}{\sqrt{\rho^2 + (x_1 - \bar{x}_1)^2 + (x_2 - \bar{x}_2)^2}}\,, \\
z_2(x) &= \frac{\rho}{\sqrt{\rho^2 + (x_1 - \bar{x}_1)^2 + (x_2 - \bar{x}_2)^2}}\,, \\
\lambda_\mu(x) &= \frac{\bar{z}(x+\mu)z(x)}{|\bar{z}(x+\mu)z(x)|}\,.
\end{aligned}
\tag{55}
$$

The parameter ρ controls the size of the instanton, and $\bar{x}$ is its center, which we always place at the lattice center: $\bar{x} = (L/2, L/2)$. Starting from the configuration (55), we performed a few cooling steps in order to smooth over the configuration at the lattice periodic boundary. After this procedure, we end up with a smooth configuration $C_0^{(1)}$ with topological charge $Q^L \approx 1$. The geometrical topological charge of this configuration is exactly equal to 1.

TABLE XII. Further results for the CP^9 model.

β	L	$\beta^2\chi_m\xi_G^{-2}$	M_G/Λ_g	$10^4\chi_t^g$	$\chi_t^g\xi_G^2$
0.7	42	0.905(20)	25.73(33)	50.5(1.1)	0.0279(9)
0.8	60	0.828(14)	23.63(25)	10.1(4)	0.0221(10)
0.85	72	0.823(12)	23.18(22)	5.1(4)	0.0213(17)
0.9	90	0.816(11)	22.88(21)	2.5(3)	0.0198(24)
0.7 *	42	0.790(8)	22.31(12)	12.3(6)	0.0179(9)
0.75 *	60	0.790(9)	22.20(17)	6.7(5)	0.0180(13)

In Fig. 9 we plot $Q(C_n^{(1)})/Q_0$, where $Q(C_n^{(1)})$ is the topological charge Q^L averaged over the ensemble $C_n^{(1)}$ for $\beta = 1.45$. We see clearly a plateau starting from $n = 8$. For $n = 10$ we also cooled the sample of configurations finding $Q^L \simeq Q_0$ after few cooling steps. This value of n is marked by a dashed line in Fig. 9. According to the above considerations, the value of Q^L at the plateau gives an estimate of $Z(\beta)$. We repeated this procedure for other values of β, checking also the dependence of the measure on the size of the instanton ρ (in the range of $\rho \sim \xi$). The behavior of $Q(C_n^{(1)})/Q_0$ is very similar to the case reported in Fig. 9 and it is superfluous to show separate figures for each value of β. The results are presented in Table XVIII. The plateaus always start from $n = 8$. On the other hand, plateaus becomes longer with increasing β.

We now proceed to the analysis of the ensembles $C_n^{(0)}$ of configurations obtained by heating the constant configuration $C^{(0)}$, defined by $z(x) = (0,1)$ and $\lambda_\mu(x) = 1$, for several values of β. In Fig. 10 we plot the average value of χ_t^L as a function of the number n of heating steps. For every value of β we observe a plateau starting from $n \simeq 24$; the plateau is longer for higher values of β, as expected. For $n = 24$ we cooled the sample of configurations and found vanishing Q^L in a few cooling steps. This value of n is marked by a dashed line in the Fig. 10. After the plateau, χ_t^L increases to reach the true equilibrium value. We identify the topological susceptibility

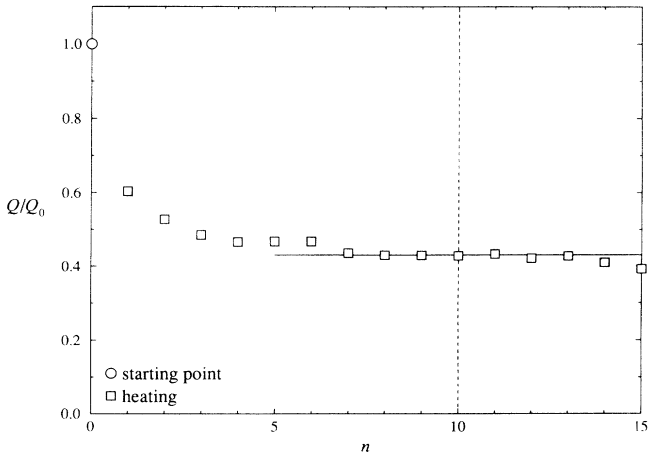

FIG. 9. Determination of the multiplicative renormalization Z for $\beta = 1.45$.

TABLE XIII. Summary of the simulation runs for the CP^{20} model. a and b denote two independent runs for the same values of β and L.

β	L	Stat	E	ξ_G	χ_m	$\tau_{int}^{\chi_m}$
0.65	24	20k m,1	0.79872(19)	2.812(23)	12.65(8)	9.9(9)
0.65	36	30k m,4	0.79926(11)	2.696(13)	12.17(3)	4.1(2)
0.65	42	40k m,1	0.79938(13)	2.703(25)	12.16(3)	3.2(1)
0.7	30	20k m,4	—	4.19(6)	21.74(25)	19.7(2.5)
0.7	36	20k m,4	0.73888(15)	3.83(3)	19.92(10)	10.9(1.0)
0.7 a	48	30k m,4	0.73923(7)	3.710(19)	19.50(4)	5.3(3)
0.7 b	48	30k m,1	0.73920(5)	3.725(26)	19.60(7)	5.1(3)
0.75	36	50k m,4	0.68639(9)	6.119(24)	37.71(15)	9.8(6)
0.75	60	40k m,1	0.68746(6)	5.12(4)	31.67(11)	6.5(3)

measured at the plateau $\chi_{t,p}^L$ with the perturbative tail at the given value of β. Since $Z(\beta)$ and $P(\beta)$ have their origin in the fluctuations at $l \sim a$, finite size corrections are of the order of L^{-2} and therefore negligible on our lattice.

Consistency of the direct measures of $Z(\beta)$ and $P(\beta)$ with the corresponding perturbative computation has been shown in Ref. [27].

The values of $Z(\beta)$ and $P(\beta)$ obtained by this procedure can be inserted in Eq. (54) to extract the physical value of the topological susceptibility ("field theoretical" method). We measured χ^L in a standard (thermalized) Monte Carlo for $\beta = 1.4$ and $\beta = 1.45$. The results are summarized in Table XIX. Scaling is observed and furthermore the value of the adimensional quantity $\chi_t \xi^2$ is consistent with the determination of Ref. [19], where a different lattice action was used.

We performed an independent measure of χ_t using the cooling method [28], which consists in measuring χ_t on an ensemble of configurations cooled by locally minimizing the action (starting from equilibrium configurations). The idea behind the cooling method is that local changes should not modify the topological properties of a configuration, and its topological content can be extracted from the cooled configuration, where the short-ranged fluctuations have been eliminated and therefore all the definitions of topological charge agree with each other and give integer values.

Our cooling algorithm consists in assigning to each lattice variable z_n ($\lambda_{n,\mu}$) a new value z'_n (λ'_n) (keeping all other variables fixed). The new value is chosen by constrained minimization of the action: we require $|z - z'|^2 \leq \delta^2$ ($|\lambda - \lambda'|^2 \leq \delta^2$) with $\delta = 0.2$. A cooling sequence was performed every 100–200 thermalization sweeps. Each cooling sequence consisted of 25 steps (a "step" is the cooling of all the lattice variables sequentially) and averages were taken at fixed cooling step across all sequences.

We used the operator $q^L(x)$ to determine the topological charge of the cooled configurations. The topological susceptibility measured on cooled configurations by Eq. (53), χ_t^{cool}, is seen to gradually rise up to an extended plateau, lasting at least the 25 sweeps performed; if we continue further the cooling procedure, the metastable structures carrying topological charge begin to disappear. Our averages and errors are estimated on the plateau measurements. They are reported in Table XIX. They are consistent with the results obtained by the field theoretical method.

VII. DISCUSSION OF NUMERICAL RESULTS

The first striking numerical evidence is that the ratios ξ_d/ξ_w and A_d/A_w show that the models defined by S_g and S_g^{Sym} enjoy perfect rotation invariance (and therefore scaling) for correlation lengths ξ as small as 2.5. This is to be compared with the CP^1 model with "standard" action, where for ξ as large as 100 it is not clear if the scaling region is reached [29, 30] (and it would be very interesting to check for rotation invariance).

The behavior of ξ_G and A_G for the CP^1 model is consistent with the notion of a correlation function saturated by one-particle states of the only existing physical particle: both ξ_G/ξ_w and A_w/A_G are consistent with 1. When we move to $N = 10$ and $N = 21$ we notice a significant decrease in both ratios, well outside statistical errors and consistent with the large-N predictions 0.816 and 0 respectively.

In the asymptotic scaling region, M_G/Λ_g must be constant and independent of the lattice action. Moreover, if our CP^1 model belongs to the universality class of the O(3) sigma model, M_G/Λ_g must tend to the asymptotic value 36.5, according to the exact result obtained in Ref. [11]. M_G/Λ_g appears to be constant within errors for the

TABLE XIV. Correlation length ξ and correlation function coefficient A for the CP^{20} model.

β	L	ξ_G	ξ_w	ξ_d	A_G	A_w	A_d
0.65	42	2.703(25)	2.86(3)	2.86(3)	4.77(4)	3.80(9)	3.81(7)
0.7 a	48	3.710(19)	3.90(4)	3.92(3)	5.53(2)	4.56(8)	4.54(6)
0.75	60	5.12(4)	5.40(7)	5.39(5)	6.53(4)	5.34(15)	5.37(10)

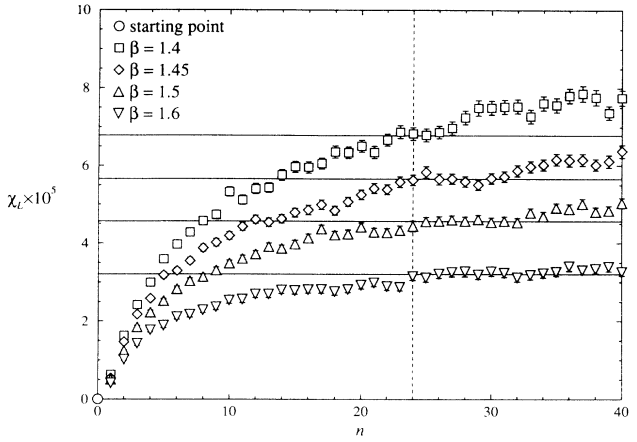

FIG. 10. Determination of the perturbative tail P of the topological susceptibility. Solid lines show the plateau values.

TABLE XV. Ratios of different definitions of correlation length and correlation function coefficient for the CP^{20} model.

β	L	ξ_G/ξ_w	ξ_d/ξ_w	A_w/A_G	A_d/A_w
0.65	42	0.944(5)	1.000(8)	0.797(17)	1.001(21)
0.7 *a*	48	0.950(4)	1.003(6)	0.824(16)	0.997(15)
0.75	60	0.947(7)	0.998(10)	0.816(26)	1.006(24)

TABLE XVI. The string tension obtained from the Creutz ratio $\chi(l,l)$ for the CP^{20} model.

β	L	l	$10^3\sigma$	$\sigma\xi_G^2$
0.65	36	8	17.0(1.4)	0.124(10)
0.65	42	8	17.7(5.4)	0.130(44)
0.7 *b*	48	11	7.5(1.6)	0.105(26)

TABLE XVII. Further results for the CP^{20} model.

β	L	$\beta^2\chi_m\xi_G^{-2}$	M_G/Λ_g	$10^4\chi_t^g$	$\chi_t^g\xi_G^2$
0.65	36	0.707(6)	19.27(9)	9.8(1.0)	0.0072(8)
0.65	42	0.702(12)	19.22(18)	11.2(9)	0.0083(9)
0.7 *a*	48	0.694(5)	19.03(10)	—	—
0.7 *b*	48	0.692(8)	18.96(13)	—	—
0.75	60	0.680(8)	18.76(15)	—	—

TABLE XVIII. Measure of the multiplicative renormalization of χ^L, starting from an instanton of size ρ.

β	L	ρ	Q_0	Stat	plateau	Z^L
1.4	48	6	0.98	500	8–10	0.40(2)
1.4	48	10	0.99	2000	8–10	0.40(1)
1.4	48	16	0.98	400	8–10	0.41(2)
1.45	48	10	0.99	1000	8–13	0.43(1)
1.5	48	10	0.99	500	8–13	0.45(1)

largest values of β in the S_g formulation. Its value (approximately 47) is far from the asymptotic one. However this is not a problem, since field theory predicts an extremely slow approach to asymptopia for quantities such as M_G/Λ_g.

For CP^9 and CP^{20} the ratio M_G/Λ_g is more stable; this is consistent with the notion that corrections to the two-loop asymptotic scaling function are depressed by a factor $1/N$. The values of M_G/Λ_g are consistent with the large-N prediction 13.86.

The rescaled magnetic susceptibility $\beta^2\chi_m\xi_G^{-2}$ is approximately constant for each of the lattice models of our study. Its behavior with respect to N is consistent with the large-N prediction 0.477.

The string tension σ is harder to measure in a Monte Carlo simulation. Our string tension results for $N = 10$ and $N = 21$ are statistically less accurate than results discussed above. Our determinations of $\sigma\xi_G^2$ are compatible with the large-N prediction π/N.

The geometrical definition of topological charge cannot be used for CP^1. We measured the topological susceptibility using the field theoretical method, which is reliable for $\xi \gtrsim 10$. We found for the action S_g values of $\chi_t\xi^2$ consistent with those obtained in Ref. [19] using the action S_1^{Sym}.

The geometrical definition of topological charge is reliable for S_g at large-N [16]. Using S_g at $N = 10$ we observed a slow approach to scaling for the quantity $\chi_t\xi_G^2$. This fact is not surprising, since scaling violations for an adimensional physical quantity defined by nonlocal operators are not bound to a $1/\xi$ behavior. The results for S_g^{Sym} are more stable and compatible with the highest β S_g results.

For CP^{20} we were able to obtain only one reliable determination of χ_t^g, due to the problem reported in Sec. III. The corresponding value of $\chi_t^g\xi_G^2$ is perfectly compatible with the $1/N$ expansion prediction (10), 0.00744 in this case. The same Eq. (10) predicts 0.0153 for CP^9, suggesting for the first neglected contribution the value $\sim 3/N^3$.

It is interesting to consider the results obtained in Ref. [31], where a lattice action obtained by analytic integration of the gauge degrees of freedom in Eq. (1) was used; numerical simulations were performed for the models at $N = 4$, 5, 6, and 8. Whenever comparisons are possible, these results interpolate smoothly between our CP^1 and CP^9 data. The models at $N = 4$ and 5 with action S_1 have been simulated in Refs. [25, 32].

Our analysis of finite size effects shows that they can be analyzed by comparing different lattice sizes L for the same value of β, obtaining finite size scaling functions that can be used to remove finite size effects systematically, extrapolating to infinite lattices. The basic point is that in this class of models, in the scaling region and for $L/\xi \gg 1$, for any physical quantity $O_L(\beta)$ measured at fixed β on a $L\times L$ lattice the following holds:

$$\frac{O_L(\beta)}{O_\infty(\beta)} \approx 1 + c_O e^{-L/\xi_{eff}(\beta,N)}, \tag{56}$$

where c_O may depend on N but not on L and β. Assum-

TABLE XIX. Measure of χ_t by the field theoretical and by the cooling method.

β	L	$10^4\ \chi^L$	$10^4\ \chi_p^L$	Z^L	$10^4\ \chi_t^{ft}$	$\chi_t^{ft}\xi_G^2$	$10^4\ \chi_t^{cool}$	$\chi_t^{cool}\xi_G^2$
1.4	120	1.35(6)	0.68(2)	0.40(1)	4.2(7)	0.11(3)	3.7(3)	0.094(17)
1.45	150	1.07(5)	0.57(1)	0.43(1)	2.7(4)	0.12(3)	2.5(2)	0.112(19)

ing Eq. (56) and evaluating c_O from best fits at intermediate values of β on reasonably small lattices leads to the possibility of extrapolating $O_\infty(\beta)$ at higher β from data on not too large lattices. Equation (56) is fully supported by numerical data for the three values of N we examined, both for $O = \xi_G$ and for $O = \chi_m$.

In the CP^1 case we observe that $\xi_{eff}(\beta) \approx \xi_w(\beta)$ and $c_{\chi_m}, c_{\xi_G} < 0$. This is the expected behavior when finite size effects are dominated by the inverse mass gap [33] ("pointlike particle within a box" effect).

In CP^{N-1} models the physical states are bound states in a linearly confining potential. Therefore their wavefunction may be nonvanishing in a range of many correlation lengths, especially at large-N where the potential is proportional to $1/N$, the binding energy to $N^{-2/3}$ and the radius of the bound state behaves like $N^{1/3}$.

It is still possible to parametrize the finite size effects according to Eq. (56) at the price of an appropriate definition of ξ_{eff}. Our numerical results for CP^9 and CP^{20} imply

$$\xi_{eff} \approx \tfrac{1}{2} N^{1/3} \xi_G \,. \tag{57}$$

This relationship reflects the N dependence on the bound state radius. Moreover the finite size function turns out to be universal (c_O is independent of N), and we observe $c_O > 0$. This unconventional sign of the finite size effect can be understood if we study the behavior of the solutions of the Schrödinger equation [2, 3] in a periodic box ("bound state within a box" effect).

VIII. CONCLUSIONS AND OUTLOOK

We think that our simulations have produced some compelling numerical evidence of the following general statements.

A properly chosen lattice action can lead to scaling for rather small correlation lengths.

Rotation invariance and stability of dimensionless ratios of physical quantities are powerful and mutually consistent tests of scaling.

Finite size scaling can be systematically used to improve the accuracy of predictions obtained on small lattices.

The standard field theory approach to renormalization of composite operators can be successfully applied to lattice-regularized models and the "heating" method described in Sec. VI and in Ref. [27] is a powerful tool in the determination of perturbative renormalization factors for topologically nontrivial quantities.

More specifically referring to CP^{N-1} models, we observe the following.

The dependence on N is rather mild and monotonic — there is no evidence for lack of convergence of the $1/N$ expansion as far as $N = 2$.

Large-N predictions are approached rather slowly, but this is consistent with the confining potential description of $1/N$ effects.

The bound-state radius predicted by the above-mentioned description is indirectly confirmed by the analysis of finite size effects.

CP^1 physics is consistent with O(3) universality and with the exact S matrix approach.

In the light of these encouraging results, we plan to extend our studies both to intermediate and to high values of N, and to increase our statistical samples enough to be able to analyze directly the properties of the bound states.

The possibility of generating accurate physical predictions in this class of models by numerical Monte Carlo methods is in our opinion a most promising signal for the usefulness and reliability of similar methods applied to four-dimensional gauge theories.

APPENDIX: GENERATION OF PROBABILITY DISTRIBUTIONS

As we noticed in Sec. III, in order to implement the heat-bath or over-heat updating algorithm for our class of models we need to generate random numbers according to the probability distribution

$$\frac{dp_k^t(\theta)}{d\theta} \equiv \rho_k(\theta) \propto (\sin\theta)^{2(k-1)} \exp(a\cos\theta) \,. \tag{A1}$$

For our purposes it is necessary to find an algorithm whose efficiency is not lost for large values of a or k. In this limit, $\rho_k(\theta)$ assumes a strongly peaked form. We devised the following algorithm.

(1) A trial variable $\bar{\theta}$ is generated according to the probability distribution

$$\rho_k^t(\theta) \propto \frac{1}{1 + c^2(\theta - \theta_0)^2} \,. \tag{A2}$$

The free parameter θ_0 is chosen equal to the value which maximizes $\rho_k(\theta)$; c is then determined by the condition

$$\frac{\rho_k^{t\prime\prime}(\theta_0)}{\rho_k^t(\theta_0)} = \frac{\rho_k''(\theta_0)}{\rho_k(\theta_0)} \,. \tag{A3}$$

The explicit formulas for the two free parameters are

$$\theta_0 = \arccos\left(\sqrt{1+\zeta^2} - \zeta\right), \tag{A4a}$$

$$c = \sqrt{2(k-1)\,\frac{1 - \zeta\cos\theta_0}{\sin^2\theta_0}} \,, \tag{A4b}$$

$$\zeta = \frac{k-1}{a}. \tag{A4c}$$

The probability distribution (A2) is Lorentzian and can be obtained directly from a uniform distribution χ in the interval $[0,1]$:

$$\bar{\theta} = \theta_0 + \frac{1}{c}\tan\left[\chi \arctan c(\pi - \theta_0) + (\chi - 1)\arctan c\theta_0\right]. \tag{A5}$$

(2) The trial variable is accepted with a probability

$$P_{\text{accept}} = \frac{\rho_k(\bar{\theta})}{\rho_k(\theta_0)} \frac{1 + c^2(\bar{\theta} - \theta_0)^2}{\eta}, \tag{A6}$$

otherwise it is rejected and we go back to step (1). η is another free parameter of the algorithm. In order to maximize the acceptance of step (2), η must be chosen (as a function of k and a) as large as possible, with the constraint that the right-hand side of (A6) must be ≤ 1 for every value of $\bar{\theta}$. If $k > 1$ we can take $\eta = 0.99$; for $k = 1$, we choose $\eta = 0.73$ for $a < 0.8$ and $\eta = 0.99$ for $a \geq 0.8$. We obtained an average acceptance of $\approx 70\%$ for CP^9 and $\approx 60\%$ for CP^{20}, both in the λ and in the z updating.

A discussion of several optimized algorithms for the generation of the distribution $\rho_1(\theta)$ can be found in [34].

[1] A. D'Adda, P. Di Vecchia, and M. Lüscher, Nucl. Phys. **B146**, 63 (1978); **B152**, 125 (1979).
[2] E. Witten, Nucl. Phys. **B149**, 285 (1979).
[3] M. Campostrini and P. Rossi, Phys. Rev. D **45**, 618 (1992).
[4] E. Rabinovici and S. Samuel, Phys. Lett. **101B**, 323 (1981).
[5] P. Di Vecchia, A. Holtkamp, R. Musto, F. Nicodemi, and R. Pettorino, Nucl. Phys. **B190**, 719 (1981).
[6] B. Berg and M. Lüscher, Nucl. Phys. **B190**, 412 (1981).
[7] K. Symanzik, in *Mathematical Problems in Theoretical Physics*, edited by R. Schrader *et al.*, Lecture Notes in Physics Vol. 153 (Springer, Berlin, 1983).
[8] P. Biscari, M. Campostrini, and P. Rossi, Phys. Lett. B **242**, 225 (1990).
[9] B. Berg, S. Meyer, I. Montvay, and K. Symanzik, Phys. Lett. **126B**, 467 (1983).
[10] R. Musto, F. Nicodemi, and R. Pettorino, Phys. Lett. **129B**, 95 (1983).
[11] P. Hasenfratz, M. Maggiore, and F. Niedermayer, Phys. Lett. B **245**, 522 (1990).
[12] M. Campostrini and P. Rossi, Phys. Lett. B **272**, 305 (1991).
[13] M. Lüscher, Nucl. Phys. **B200** [FS4], 61 (1982).
[14] G. Martinelli, R. Petronzio, and M. A. Virasoro, Nucl. Phys. **B205** [FS5], 355 (1982).
[15] D. Petcher and M. Lüscher, Nucl. Phys. **B225** [FS9], 53 (1983).
[16] P. Di Vecchia, R. Musto, F. Nicodemi, R. Pettorino, and P. Rossi, Nucl. Phys. **B235** [FS11], 478 (1984).
[17] B. Berg and P. Panagiotakopoulos, Nucl. Phys. **B251** [FS13], 353 (1985).
[18] B. Berg, Phys. Lett. **104B**, 475 (1981).
[19] A. Di Giacomo, F. Farchioni, A. Papa, and E. Vicari, Phys. Rev. D (to be published).
[20] M. Lüscher, Phys. Lett. **78B**, 465 (1978).
[21] R. Petronzio and E. Vicari, Phys. Lett. B **254**, 444 (1991).
[22] M. Creutz, Phys. Rev. D **36**, 515 (1987).
[23] S. Adler, Phys. Rev. D **37**, 458 (1988).
[24] N. Madras and A. D. Sokal, J. Stat. Phys. **50**, 109 (1988).
[25] M. Hasenbusch and S. Meyer, Phys. Rev. Lett. **68**, 435 (1992).
[26] M. Campostrini, A. Di Giacomo, and H. Panagopoulos, Phys. Lett. B **212**, 206 (1988).
[27] A. Di Giacomo and E. Vicari, Phys. Lett. B **275**, 429 (1992).
[28] M. Teper, Phys. Lett. B **171**, 81 (1986); **171**, 86 (1986).
[29] P. Hasenfratz and F. Niedermayer, Nucl. Phys. **B337**, 233 (1990).
[30] U. Wolff, Nucl. Phys. **B334**, 581 (1990).
[31] A. C. Irving and C. Michael, Liverpool Report No. LTH 268, 1991 (unpublished).
[32] K. Jensen and U. J. Wiese, Nucl. Phys. **B370**, 762 (1992).
[33] M. Lüscher, Phys. Lett. **118B**, 391 (1982).
[34] H. Nakajima, in *Lattice '91*, Proceedings of the International Symposium, Tsukuba, Japan, 1991, edited by M. Fukujita *et al.* [Nucl. Phys. B. (Proc. Suppl.) (in press)].